# Deformation Resistance in Oriented Nylon 6

**L. Lin and A. S. Argon***

*Department of Mechanical Engineering, Massachusetts Institute of Technology, Cambridge, Massachusetts 02139*

*Received January 13, 1992; Revised Manuscript Received April 6, 1992*

ABSTRACT: Initially spherulitic nylon 6 was textured into a quasi-single crystal form by plane-strain compression at 170 °C in a deep channel-die to a compression ratio of 4.0, followed by cooling under pressure to room temperature. The resulting material, having orthotropic symmetry with quasi-single crystalline perfection, had a dual morphology in which the normals of the crystallographic (100) planes equipartition at ±21° with respect to the constraint direction of the plane-strain deformation. This highly textured material, having relatively large dimensions in all directions, was used to study the elastic and plastic anisotropy of the actual constituent lamellar crystallites. As a result, a complete set of nine elastic compliances of the orthotropic sample were measured by a simple direct technique and were related to the monoclinic crystal properties. In addition, detailed measurements were made of the plastic anisotropy of this textured material to establish that plastic response of the actual monoclinic nylon 6 crystallites is derived principally from three crystallographic slip processes consisting of the (001)[010] and (100)[010] chain slip systems and the (001)-[100] transverse slip system. The plastic shear resistances of all these slip systems were found to increase substantially with increasing compressive stress acting across the slip planes. Among these three deformation mechanisms, (001)[010] chain slip is the easiest system to be activated.

## I. Introduction

Many semicrystalline polymers are sufficiently ductile to undergo large plastic strains by extensional flow in tension or compression resulting in anisotropic end products of very attractive mechanical properties.[1,2] It is now well appreciated that while all semicrystalline polymers are made up of amorphous and crystalline components, roughly of equal proportion, it is the plastic properties of the crystalline component that govern the overall deformation behavior and the symmetry of the lattice that establishes the final anisotropic properties. Much of the previous understanding of the deformation process in such polymers had been based on kinematical arguments of the crystal plasticity accompanied by some macroscopic measurements. Presently, however, fundamental developments in the simulation of plastic flow of polycrystalline aggregates of metallic solids[3] also permit the simulation of large strain plastic flow of semicrystalline polymers as corresponding aggregates of chain-folded lamellar crystallites and intervening amorphous layers,[4] provided the anisotropic plastic resistances of the crystalline component can be given, together with those of the amorphous component. For semicrystalline polymers, this information is seriously deficient, first, because the chain-folded crystallites are far too small to permit any meaningful measurements and, second, because their form of aggregation into spherulites makes any form of analysis of measurements and attribution of component resistances to mechanisms nonunique. Young and Bowden[5] were the first to note that when such polymers were deformed in extensional flow of plane-strain compression to very large compression ratio, the resulting highly textured material resembles closely a macroscopic single crystal of the actual crystalline component or a quasi crystal version having many of the same symmetry properties of the actual crystallites. Moreover, the anisotropic plastic properties of these quasi crystals can provide very valuable information on the actual crystallographic slip resistances of the lamellar crystallites. Such information can then be used in computer models of plastic flow and texture evolution of the type developed by Ahzi et al.[4] Here we will present the results of such measurements performed on quasi-crystalline nylon 6 having orthotropic symmetry, made up of two sets of symmetrically arranged monoclinic crystallites, mixed intimately in a dual microstructure.

Undeformed nylon 6 has a spherulitic morphology.[6] Usually, three or four nearest-neighboring lamellae have the same tangentially-random orientation. The SAXS long period between lamellae is about 100 Å. The width of lamellae is in the range 150–600 Å. The longest lamellae can be followed from the center to the border of a spherulite. Nylon 6 crystals can exist in two major forms: monoclinic $\alpha$[7-10] and monoclinic $\gamma$,[11-13] although the existence of other structures has also been reported.[14] The two forms usually coexist in the bulk material. The principal differences of these two forms are in the lattice parameters and the orientation of the hydrogen bonds between the NH and the C=O groups. In the $\alpha$ phase, the hydrogen bonds are formed in the zigzag planes and between antiparallel chains. In the $\gamma$ phase, the molecular chains have to twist away from the zigzag planes to form the hydrogen bonds between parallel chains. This twisting of molecules results in a slight shortening of the periodicity in the chain direction. The $\alpha$ phase can be converted to the $\gamma$ phase by iodine treatment,[12] and the $\gamma$ phase can be converted to the $\alpha$ phase by phenol treatment[15] and by stretching.[16] The $\alpha$ phase has been found to be the most stable structure of nylon 6 crystals.[17] Figure 1 illustrates the respective structures of the two forms of crystals.

At very small strain, the response of the material is linear elastic. This behavior is described by a set of elastic constants of the material. No complete set of elastic constants has been experimentally measured for either monoclinic nylon 6 crystals or textured nylon 6 with orthorhombic symmetry.[18,19] The multiplicity of crystal phases and the lower symmetry of the crystals make it more difficult to obtain uncoupled and complete information about the anisotropic elastic property of nylon 6 on the crystallographic level.

Above a critical resolved shear stress, polymers undergo plastic deformation. This occurs up to substantial levels of strain by a combination of crystallographic slip and in some cases also by mechanical twinning and stress-induced martensitic transformation.[20] These mechanisms are similar to those occurring in many other inorganic crys-

0024-9297/92/2225-4011$03.00/0 

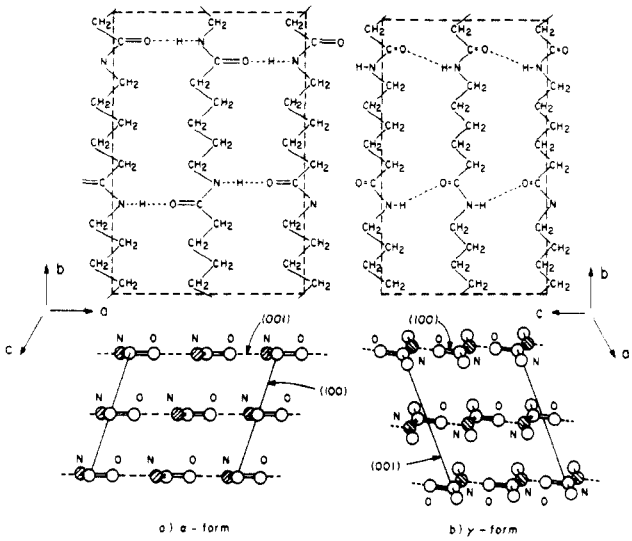


**Figure 1.** Two views of the crystal structures of nylon 6: (a) $\alpha$ form; (b) $\gamma$ form.

talline materials. Experiments on polyethylene[21-28] have established that crystallographic deformation occurs on the (100)[001], (010)[001], (110)[001], (010)[100], (100)-[010], and (110)[110] slip systems and the (110) and (310) twinning systems for this material with orthorhombic structure. The occurrence of stress-induced martensitic shear transformation from the orthorhombic to the monoclinic lattice in polyethylene was also detected by X-ray studies.[29] For polymers with a more complicated crystal structure, such as nylon 6 that is of interest here, there is little information on the deformation behavior on the crystallographic scale.

To study the properties of individual deformation systems of crystals and to obtain quantitative information, it is desirable to work on single crystals. Unfortunately, because of the size of the individual lamellar crystals, this is realistically not possible. Nevertheless, some studies were indeed undertaken on some polymer single crystals stretched on flexible substrates in the electron microscope,[30,31] but little quantitative information has resulted that is of any relevance to the deformation of the material in bulk. Therefore, as we have already discussed above, it is much more attractive to experiment on highly textured bulk material that has the perfection nearing that of a quasi-single crystal, albeit with intervening amorphous layers. Studying the mechanical behavior on such a macroscopic scale is not only more relevant to the deformation of the bulk material but also much easier to perform, since relatively large-size samples can be made having the simple and well-organized morphologies similar to the actual crystallites.

Thus, the purpose of the present research has been to develop such large-size bulk samples of semicrystalline polymers with a well-defined and simple quasi-single crystal morphology that can be readily used to measure a complete set of elastic constants of the highly textured nylon 6, to identify the principal crystallographic plastic deformation mechanisms of the material, and to determine the anisotropic yield conditions associated with each deformation mechanism. The present research constitutes a further increment on our previous studies on the morphology,[6] mechanical properties,[32] and, particularly, large strain-induced texture development[33,34] in nylon 6.

## II. Experimental Procedure

**2.1. Starting Material.** The material used in this study was nylon 6 (Capron 8200 extracted, Allied Corp.). The weight-average molecular weight $M_w$ of the material was 32 600, and the polydispersity ratio ($M_w/M_n$) was 1.80, using trifluoroethanol as the mobile phase in the measurement. The material was compression molded into small plates having dimensions of 12.7 mm thickness, 76.2 mm width, and 127 mm length. The plaques were annealed at 170 °C in vacuo for 1 day before put in use.

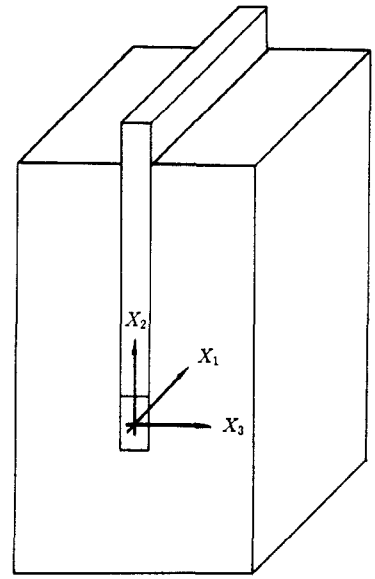


**Figure 2.** Schematic view of the deep channel-die used for obtaining highly textured polymers.

**2.2. Preparation of Highly Textured Polymers.** Plastic deformation under so-called radial loading, preserving the ratio of strain increments, results in the evolution of pronounced deformation textures. This is a result of systematic lattice rotations that accompany crystallographic slip processes. Thus, a very large plastic strain converts the originally random orientation of lamellar crystals of complicated morphology into a well-defined and simpler form. By such monotonic large strain deformation, bulk polyethylene with dual texture[35,36] and single texture[5,37-39] and nylon 6 with dual texture[18,19] were obtained by different modes of deformation. These techniques involved (a) a combination of cold drawing and rolling, followed by annealing,[21,35,37] (b) biaxial drawing,[36] (c) heave rolling followed by annealing,[38,39] (d) plane-strain compression ina channel-die,[5] and (e) drawing, annealing, and slight rolling after annealing.[18] It should be pointed out, however, that, in the early studies, the well-oriented materials obtained were usually rather small in at least one dimension, which imposed limitations on the subsequent micromechanical experiments.

A deep channel-die apparatus was designed and built to perform large plane-strain deformation and obtain well-textured samples with a relatively large size in all dimensions. Figure 2 gives a schematic view of the central part of the apparatus. The shape of the die is similar to the one used by Young and Bowden.[5] The outside dimensions of the die were 76.2 mm (length), 76.2 mm (width), and 127 mm (height), while the depth and width of the actual channel were 76.2 and 10.5 mm. For ready reference, we will abbreviate the free plastic flow direction, the loading direction, and the constraint direction as FD, LD, and CD in what follows and choose the axes $X_1$, $X_2$, and $X_3$ parallel to these directions. A heating system was attached to the die so that compression texturing of polymers can be done at any desired high temperature to reduce the deformation resistance and increase the ductility of the material being compressed. Other reinforcing parts were also added to the die to assure overall stiffness and strength.

The material to be textured was machined to have a thickness of 10.45 ± 0.05 mm to fit snugly into the slot of the die to prevent lateral deformation. The surfaces of the sample in contact with the die and plunger were lubricated with molybdenum disulfide powder. A typical run for nylon 6 started with heating the die and the sample up to 170 °C and maintaining the temperature for 3 h for equalization. The sample was then compressed in the die by slowly applying 500 000$g$ load increments through a 200-

ton hydraulic press controlled by a personal computer system. After a desired compression ratio was reached, heating was stopped, and the sample was allowed to cool down to room temperature under the maximum compression load. To improve the crystallinity,[40,41] the crystal perfection, and the stability,[14] the compressed material was annealed in vacuo at 195 °C for 24 h. This was found to be the optimum temperature for nylon 6.[18] During annealing, the sample was confined in a special fixture designed to reduce shrinkage and maintain the texture of the oriented material. Such annealing also minimizes loss of orientation in the amorphous materials.[42,43]

**2.3. Characterization of the Textured Nylon 6.** The densities of nylon 6 were measured at 21 °C by using a density gradient column made up of a mixture of toluene and carbon tetrachloride. The column was calibrated by a set of density marker floats. The samples used were cube-shaped chips with sides of about 3 mm. The readout of the sample position was made 15 min after the samples were introduced into the column to assure that equilibrium had been reached.

The structure and orientation distributions of the crystals in the highly textured nylon 6 samples were studied by wide-angle X-ray scattering (WAXS). The WAXS measurements were performed by means of a Rigaku WAXS system with pole figure attachments. The system was controlled by a microVAX computer running DMAXB Rigaku software. Cu K$\alpha$ X-rays were generated from a rotating-anode point source operating at 50 kV and 60 mA and filtered using electronic filtering and the appropriate thin Ni filter. Specimens for WAXS measurements had dimensions of 10 mm × 10 mm square and 1 mm thickness. Three specimens with different orientations were prepared for the WAXS intensity vs $2\theta$ measurements. The flat surfaces of the specimens, cut out from oriented samples, were perpendicular to FD, LD, and CD, respectively. The scanning angle $2\theta$ ranged from 10° to 85° with 0.5° steps. The scanning speed was 2°/min. For pole figure measurements, the flat surface of the specimen was perpendicular to FD. Complete pole figures for Euler angle $\alpha$ ranging from 0° to 90° with 5° steps and $\beta$ from 0° to 360° with 5° steps were obtained by combining the X-ray data from the transmission and reflection modes. The connecting angle was 50° for $2\theta$ less than 50° and 30° for larger angles.

The morphology of lamellar crystals in the highly textured nylon 6 was studied by 2D small-angle X-ray scattering (SAXS). Measurements of SAXS were performed by means of another Rigaku X-ray system consisting of a rotating-anode X-ray generator and a Nicolet 2D position-sensitive X-ray detector. The X-ray generator was operated at 40 kV and 30 mA. The specimens for SAXS measurements were the same as those for WAXS measurements. The primary beam of the SAXS system was collimated by a special two-mirror collimator. The distance between a specimen and the X-ray detector of the SAXS system was 110 cm. The enclosed pathway of scattered X-rays between a specimen and the detector was filled with He gas to minimize attenuation and background scattering.

**2.4. Elastic Anisotropy Measurements.** The oriented semicrystalline polymers are elastically highly anisotropic. A minimum of nine elastic constants are required to fully characterize the elastic behavior of the textured nylon 6 having an orthotropic symmetry (see section 3.1). The material principal axes are parallel to the $X_1$, $X_2$, and $X_3$ axes of the channel-die coordinate system. In the present work, a set of nine compliances, as referred to the three principal axes, was measured at room temperature by direct uniaxial compression experiments.

Parts a–c of Figure 3 illustrate the experiments for determining the compliances $S_{11}$ and $S_{12}$, $S_{22}$ and $S_{23}$, and $S_{33}$ and $S_{13}$, where the applied stresses are parallel to the $X_1$, $X_2$, and $X_3$ axes, respectively. Specimens were cut from textured nylon 6 and machined to rectangular parallelepiped shapes. The dimensions of the spcimens were 10.5 mm in the loading direction and 7.0 mm each in the two transverse directions. As an example, consider the $S_{11}$ and $S_{12}$ measurements. A set of two strain gauges (CEA-06-062WT-350) was glued on the $X_3$ plane face. The glue used was M-Bond AE-10 adhesive. Both the strain gauges and the adhesives were purchased from Measurements Groups, Inc. The strain gauges were oriented in a way, where one gauge measured the strain $e_{11}$ and another the strain $e_{22}$. Compression tests were performed on an Instron (Model 1125) machine. Data in the form of applied load and strains were collected through a Keithly Series 500 measurement and control system. The applied stress $\sigma_a$ is defined by

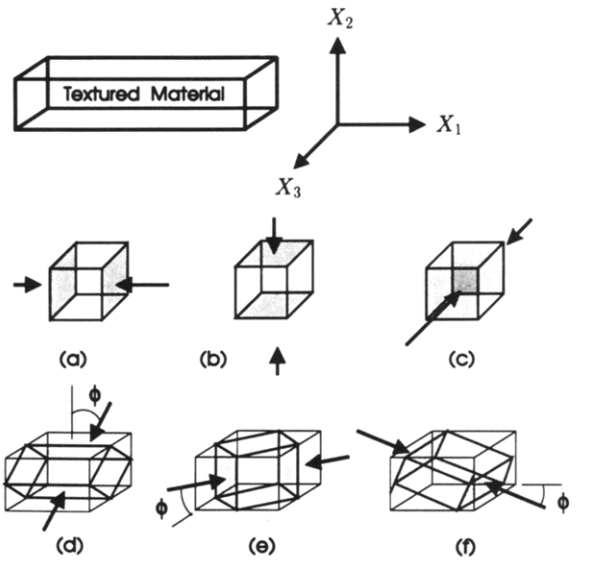


**Figure 3.** Schematic view of the sample preparation for the experimental determination of the elastic compliances of textured nylon 6.

$$\sigma_a = P/A_0 \tag{1}$$

where $P$ is the applied load and $A_0$ is the initial cross-sectional area of a specimen. To be certain that the applied stress was evenly distributed on the compressed samples, the tests were performed in a compression die which had two nearly perfectly parallel plane surfaces and was very rigid. The contact surfaces between the specimens and the die were lubricated by silicone grease (Dow Corning 33) provided by the Dow Corning Corp. During motion of the cross-head of the machine, down at a velocity of 0.125 mm/min, strains $e_{11}$ and $e_{22}$ were measured intermittently as a function of the applied stress $\sigma_a$. The slopes of the "best fit" straight lines to the $e_{11}$ and $e_{22}$ data as a function of $\sigma_a$ were taken as the compliances $S_{11}$ and $S_{12}$.

To measure shear compliances $S_{44}$, $S_{55}$, and $S_{66}$, shear stresses have to be imposed on corresponding planes and in corresponding directions. This was achieved by preparing samples in such a way that the loading direction was normal to one principal material axis and inclined to the other two principal material axes. For the sake of simplicity, the angles $\phi$ of inclination were chosen to be 45°. The shape of these samples was cuboid, and the dimensions were 9.5 mm in the loading direction and 6 mm in the transverse directions. Parts d–e of Figure 3 illustrate how the experimental samples were prepared for the three shear compliances $S_{44}$, $S_{55}$, and $S_{66}$. As an example, consider the measurement of $S_{44}$ by the relation

$$S_{44} = \mathrm{d}e_4/\mathrm{d}\sigma_4 \tag{2}$$

where $e_4$ is the shear strain defined by

$$e_4 = \gamma_{23} = 2\epsilon_{23} = \frac{\partial u_2}{\partial x_3} + \frac{\partial u_3}{\partial x_2} \tag{3}$$

and $\sigma_4$ is the corresponding shear stress

$$\sigma_4 = \sigma_{23} = \frac{1}{2}\sigma_a \tag{4}$$

because the angle $\phi$ was taken to be 45°. A set of three strain gauges (WK-03-060WR-350) was glued onto the $X_1$ surface with one in the $X_2$ direction, one in the $X_3$ direction, and one perpendicular to the loading direction. The corresponding strains measured were labeled as $e_A$, $e_C$, and $e_B$. The shear strain $e_4$ was obtained from

$$e_4 = 2e_B - (e_A + e_C) \tag{5}$$

according to a simple analysis. The data of $e_4$ vs $\sigma_4$ were then fitted by a best fit straight line, and the slope of the line was

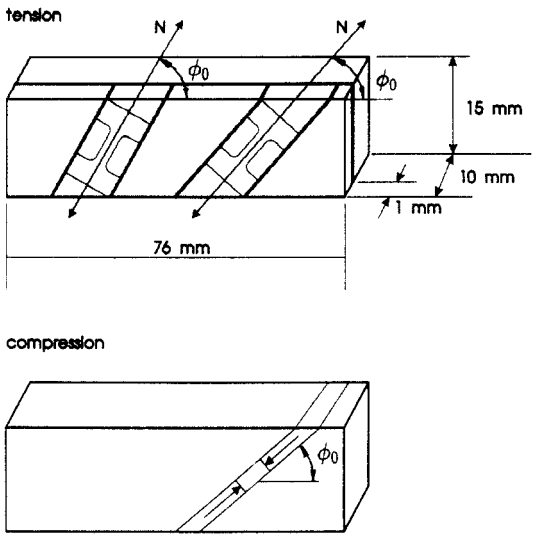


**Figure 4.** Schematic view of the sample preparation for the experimental determination of the yield condition of the (001)-[010] crystallographic slip.

taken as the compliance $S_{44}$. In a similar way, the shear compliances $S_{55}$ and $S_{66}$ were determined.

**2.5. Plastic Anisotropy Measurements.** To quantitatively determine the plastic anisotropy of oriented semicrystalline polymers and attribute it to different deformation mechanisms, special tests were devised so that the behavior of each possible deformation mode became measurable. For best results, only one deformation mode, such as a specific crystallographic slip system, should be activated during one test. Other competitive modes of deformation should remain dormant. On the other hand, the mechanical tests should also be able to impose different combinations of resolved shear stress and normal stress to each possible deformation mode to determine the normal stress sensitivity of the plastic shear resistance.

From X-ray analysis, the structure, morphology, and texture of the oriented nylon 6 can be accurately determined as we will present in section 3.1. The crystallographic deformation modes can be determined by relating the deformation increments to the crystal structure as will be presented in section 3.2. The principal plastic deformation mechanisms for nylon 6 are the (001)[010], (100)[010], and (001)[100] crystallographic slip processes. Specimens for uniaxial tension tests and uniaxial compression tests were prepared in special relationship to the structure and morphology of the highly textured nylon 6 samples. Figure 4 illustrates how the specimens were cut from the textured material for studying the (001)[010] slip, where the [010] slip direction and applied stress direction form an angle $\phi_0$, and these two directions and the (001) slip-plane normal are in a same plane. For a different initial angle $\phi_0$, a different combination of resolved shear stress and resolved normal stress could be imposed to activate the (001)[010] slip system. For the (100)[010] and (001)-[100] slips, specimens were prepared in the same way but with different orientations. Table I lists the initial angle $\phi_0$ for experiments determining the yield conditions associated with the (001)[010], (100)[010], and (001)[100] slip systems. Experiments were also performed with the angle $\phi_0$ chosen to lie outside the ranges given in Table I. But, in these cases, there was evidence that more than one deformation system was involved in such tests. Therefore, the results are difficult to interpret and will not be discussed here.

The specimens were cut from oriented material by means of a milling machine, taking special care to prevent damage to the existing texture and morphology of the material. Marks were drawn on the specimens to indicate the expected slip directions and slip planes for verifying of the deformation modes after tests. For tension experiments, the specimens had a dumbbell shape. For compression experiments, the specimens had a cuboid shape. The effective gauge lengths of the specimens for both tension and compression were prepared based on the magnitude of the angle $\phi_0$ to assure that the shear in the expected direction occurs within the gauge section in an unhindered manner. Both tension and compression experiments were performed on an Instron 4201 machine at an initial strain rate of 0.1/min.

**Table I**
**Initial Angles between Applied Loads and Slip Direction for Yield-Locus Determination**

| $\phi_0$ (deg) | (001)[010] | (001)[001] | (100)[010] |
|---|---|---|---|
| | Tension | | |
| 25 | √ | | |
| 35 | √ | | √ |
| 45 | √ | | √ |
| 55 | √ | | √ |
| 65 | √ | | √ |
| | Compression | | |
| 25 | √ | | √ |
| 35 | √ | √ | √ |
| 40 | | √ | |
| 45 | √ | √ | √ |
| 50 | | √ | |
| 55 | √ | √ | √ |

To be certain that only one system was initially activated in each individual test, the samples were examined immediately after the tests. If slip occurs only in a direction perpendicular to the thickness direction of the sample, there should be no change in thickness. For tension experiments with a 10% engineering plastic strain in the tensile direction, the reduction of thickness of samples was not measurable by a micrometer for all tests for the three deformation modes. For compression experiments with a 10% plastic strain in the compression direction, some increase of thickness could be measured with a micrometer, but the calculated strains in the thickness direction were found to be less than 0.5%. Therefore, the deformations must have occurred in a direction normal to the thickness direction of the samples as desired, and the small transverse strain was attributed to end effects.

When the fully developed plastic deformation was not very large, the exact shear direction could not be easily identified by simply examining the geometry of the samples used. To further check the shear direction, samples were loaded to points where the loads started to drop, i.e., to where the deformations became unstable. The tension samples deformed to such points clearly exhibited well-defined but somewhat diffuse shear bands in the expected slip directions, as shown in Figure 5 for the (100)[010] slip, for example. This indicates that slip occurred and concentrated in the expected directions. For compression experiments, the samples after being deformed to the points of deformation localization showed shapes as illustrated in Figure 6. Such a shape is, most likely, caused only by concentrated shear in the expected slip directions.

**2.6. Humidity Control.** It has been well-known for some time that the mechanical properties of nylon 6 are very sensitive to the level of water absorbed by the material.[32,44-46] The plastic resistance of nylon 6 can drop to as low as $^1/_3$ of its originally "bone-dry" material value, when it becomes saturated with water.[32,46] The decrease in the strength is approximately directly proportional to the amount of water absorbed. To study the mechanical properties of nylon 6 without the interference of its strong moisture dependence, the water content in the samples to be tested had to be controlled to a constant reference level.

Penetration of water into nylon 6 does not occur in a simple Fickian manner for which the characteristic times, for known conditions, can be readily predicted for an environment with a given constant humidity and temperature but is rather of a, so-called, case II type. In this form of diffusion, the penetrated water swells the surface layer of the material and results in compressive stresses that act as a barrier for further penetration, which, in turn, changes the diffusion pattern. Removal of water from nylon is even more complicated. There are two types of interaction with water of concern in nylon 6.[47-52] One interaction is referred to as loosely bound water, which can be removed by desiccation. The other is called tightly bound water, which can be removed only by heating in a vacuum for several days. Thus, it is very difficult to obtain samples with a specific content of water and maintain the same content for a long time.

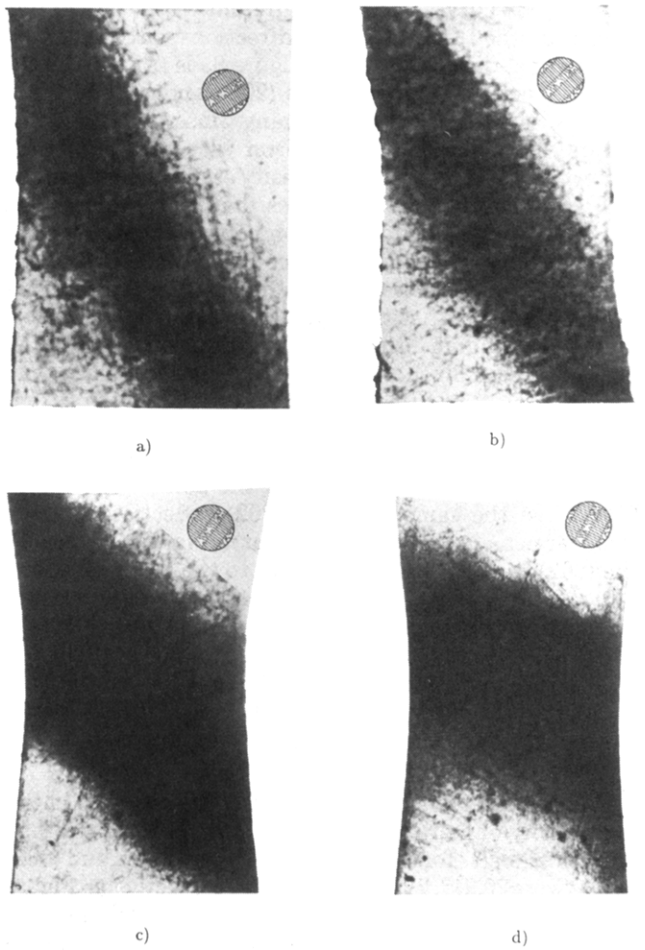


**Figure 5.** Photographs of deformed tensile samples for the (100)-[010] slip to show the shear bands along the chain direction: (a) $\phi_0 = 35°$; (b) $\phi_0 = 45°$; (c) $\phi_0 = 55°$; (d) $\phi_0 = 65°$.

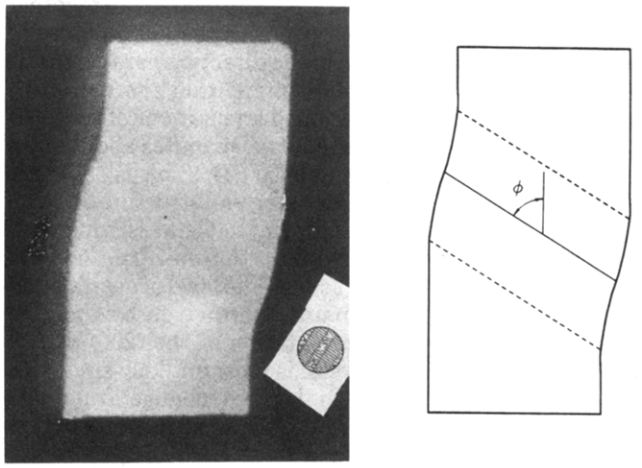


**Figure 6.** Photograph and schematic representation of a deformed compression sample.

On the other hand, for reasons stated above, the diffusion of water into nylon 6 is a very slow process. In samples of bulk proportions the effect of humidity under ambient conditions is not felt in a relatively short time.[53,54] For instance, the equilibration time for samples of 0.25 mm thickness was found to be about 5 days at 20 °C for a wide range of relative humidity.[18,54] Thus, it is possible to maintain the water content in nylon 6 at its original level for periods of time that are long enough for reproducible results in the mechanical study. In the present case, the smallest dimension of all samples or specimens was in excess of 1.0 mm. Since a certain level of water content imparts to nylon its desirable tough properties, it was decided to study its mechanical properties in such an intermediate state that was neither bone-dry nor fully saturated. To achieve reproducibility, the compression-molded samples were kept in hermetically sealed "Ziplock" bags most of the time. After the materials were oriented by plane-strain compression, in the form of blocks of dimensions 76 mm × 15 mm × 10 mm and annealed in vacuum, the overall time of exposure to the environment for its preparation and testing was not more than 5 h. In this way, the water content of the samples can be assumed to be maintained at a nearly constant reference level.

**Table II**
**Density and Crystallinity of Nylon 6**

| compression ratio | density (Mg/m³) | crystallinity (%) | |
|---|---|---|---|
| | | *a* | *b* |
| 1.0 | 1.145 | 38.5 | 44.3 |
| 4.0 | 1.151 | 43.4 | 52.2 |

[a] Present work. [b] Reference 33.

## III. Results and Discussion

**3.1. Textured Nylon 6 Obtained from Plane-Strain Compression.** The textured nylon 6 used in the mechanical anisotropy study presented below had a compression ratio between 3.8 and 4.0. Although more highly textured materials could be obtained, they were too brittle in the transverse direction for further deformation studies of anisotropic yielding behavior.

The densities of nylon 6 in both untextured and textured form with a compression ratio equal to 4 are listed in Table II. The volume fractions $\chi$ of the crystalline component were estimated from

$$\chi = \frac{\rho - \rho_a}{\rho_c - \rho_a} \tag{6}$$

where $\rho$, $\rho_c$, and $\rho_a$ are the densities of the overall material, the crystalline portion, and the amorphous portion of nylon 6, respectively. As collected by Lewis and Ward[18] from 18 groups of investigators, the crystalline density ranges from 1.208 to 1.235 Mg/m³, and the amorphous density, from 1.079 to 1.150 Mg/m³. Thus, there is some uncertainty about the exact values. The mean value 1.22 Mg/m³ for crystalline density and 1.098 Mg/m³ for amorphous density were used in our calculations of the crystallinities. The results of the calculations are given in the Table II. The crystallinities of the same materials were also calculated from X-ray diffraction data using the overlapping peaks deconvolution technique[33] followed by integration. The X-ray results are also listed in Table II. In comparing the findings, the estimates from density measurements are generally lower than those from X-ray measurements. Regardless of the methods used, the data show that the crystallinity is increased due to the plane-strain compression in the channel-die.

Changes of the diffracted intensity of WAXS with the Bragg angle $\theta$ were measured for untextured and textured nylon 6. Figure 7 is the plot of intensity vs $2\theta$ for the untextured material that can be considered as a randomly oriented polycrystalline "powder". Parts a–c of Figure 8 are the diffracted intensity plots for textured material, with the respective $X_3$, $X_2$, and $X_1$ directions being the bisectors of the angles between the incident beams and the diffracted beams. The $2\theta$ values at the peaks in Figure 8 are listed in Table III. Without a detailed intensity analysis, the corresponding reflection planes can be easily recognized by comparing these diffraction angles with the early findings of other investigators. The 69° value of the crystallographic angle $\beta$ between $a$ and $c$ in Table III is determined from WAXS pole figures which will be discussed shortly. The other lattice parameters of the

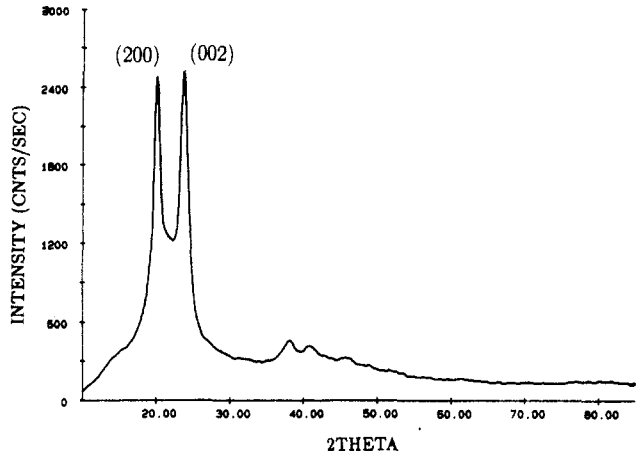


**Figure 7.** Intensity vs $2\theta$ curve of wide-angle X-ray scattering from untextured nylon 6.

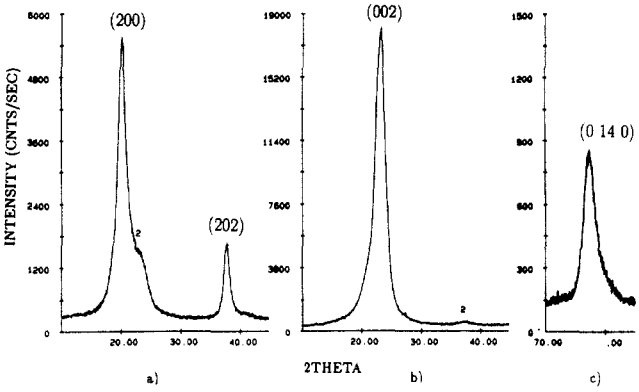


**Figure 8.** Intensity vs $2\theta$ curve of wide-angle X-ray diffraction from textured nylon 6: (a) scanning in the $X_1X_3$ plane and around the $X_3$ direction; (b) scanning in the $X_1X_2$ plane and around the $X_2$ direction; (c) scanning in the $X_1X_3$ plane and around the $X_1$ direction.

nylon 6 crystals were calculated based on the $2\theta$ values and the $\beta$ value and are also listed in the table.

Comparing the reflection angles and the lattice parameters of our textured material with the results of others in Table III reveals that the predominant crystals in the textured material are in the $\alpha$ form, although very small volume fractions of $\gamma$ crystals may also exist as shown by the slight shoulder in the main peak in Figure 8a. The predominance of this particular crystalline form comes from the original untextured material and the large plastic deformation. The $\gamma$ form of nylon 6 crystals can transform to the $\alpha$ form by stretching in the chain direction.[16] The plane-strain compression in the LD is geometrically equivalent to stretching in the FD while keeping the material at a constant length in the CD. The plane-strain compression resulted in some elongation of the $b$-axis, which is parallel to the FD, and some shrinkage of the $c$-axis, which makes an acute angle with the LD. These changes of lattice parameters were accompanied by rotation of the hydrogen bonds from (200) planes (of the $\gamma$ phase) to (002) planes (of the $\alpha$ phase).

Comparison of the intensity plot in Figure 7 and those in Figure 8 suggests that the plane-strain-compressed material has been well textured, with the (002) plane normals rotating toward the LD, the (0 14 0) plane toward the FD, and the (200) plane toward the CD. For the original untextured material, the intensity vs $2\theta$ curves were the same no matter from what direction the samples were examined by X-rays. The reflections of (002) planes and (200) planes unavoidably overlapped each other as shown in Figure 7. For the compressed material, the intensity–$2\theta$ curves were very different when the samples were examined from different directions with respect to the channel-die coordinates. Figure 8a is principally the (002) reflections, Figure 8b the (200), and Figure 8c the (0 14 0). Some peaks became many times stronger, while others disappeared in comparison with the unoriented material. For instance, the intensity of the (002) reflection in Figure 8b was about 7.5 times that in Figure 7, while the peak for the (200) reflection could not be detected. The intensities from (200) planes and (002) planes of the untextured material were about the same as seen in Figure 7, which implies that the crystals of the material have a uniformly-random orientation distribution. The (002) peak in Figure 8b shows a much stronger intensity than the (200) peak in Figure 8a. The reason for this is that the (002) plane normals distribute around the LD, but the (200) plane normals distribute about a direction 21° away from the CD, as will be shown by the pole figures which follow. In the same way, the ($\bar{2}$02) reflections show a stronger peak in Figure 8a than that in Figure 8b, because the ($\bar{2}$02) plane normals are closer to the LD than to the CD. Figure 7 shows that the (0 14 0) reflection was not measurable in the original undeformed material. This is due to a low atomic scattering factor for the (0 14 0) planes. But for textured material, the (0 14 0) peak is well-defined, as can be seen in Figure 8c. This is because there is now a high concentration of (0 14 0) planes that contribute to the reflection intensity.

The pole figures of the diffracted X-ray intensity of the textured nylon 6 are presented in Figure 9a–c. The Bragg reflection angles for (200) planes, (0 14 0) planes, and (002) planes were 20.21°, 77.42°, and 23.09°, respectively. Figure 9a indicates that the (002) plane normals distribute very closely around the LD of the channel-die. Figure 9b indicates, in turn, that the (0 14 0) plane normals distribute very closely around the FD. Since the lamellar crystals of the compressed nylon 6 are predominantly in the $\alpha$ form as discussed earlier, parts a and b of Figure 9 together make it clear that hydrogen bonds in the (002) planes of the material are aggregated in the direction parallel to CD of the channel-die. Figure 9c shows that there are two possible symmetrically positioned orientations of the (200) planes. One set of plane normals distributes about +21° to CD and the other about −21° to CD. This is expected from the nature of the monoclinic crystal structure of nylon 6. The intensity contours indicate that the assignment of the (200) planes to the two orientations is about equally divided at the macroscopic scale. The level of aggregation of the (200) planes in domains is not given by the pole figure. Clearly, the dual orientation of the (200) planes within a single lamellar crystal is most unlikely since this would result in gaps when lattices change from one orientation to another and requires a significant reduction in density. But since there is no reason for any preference of the two orientations of lattices for a particular lamellar crystal, both orientations appear with equal frequency. From Figure 9c, the crystallographic angle between the $a$-axis and the $c$-axis was determined to be 69°.

The shape and orientation distribution of lamellar crystals were studied by SAXS. Figure 10 shows the SAXS patterns of nylon 6 textured by plane-strain compression. When the X-ray beam was incident on the sample in the direction parallel to the LD of the channel-die, the SAXS pattern (Figure 10a) showed two concentrated maxima which can be interpreted in the traditional way, that the edges of lamellar crystals are straight, with the flat amorphous layers being perpendicular to the FD. Furthermore, the distance of the lamellar long spacings in the

**Table III**
**Summary of Lattice Parameters and Major Reflection Angles of Nylon 6**

| type | $a$ (Å) | $b$ (Å) | $c$ (Å) | $\beta$ (deg) | $2\theta$ (deg) ($\lambda$ = 1.542) (200) | (0 14 0) | (002) | (20$\bar{2}$) | (202) | ref |
|---|---|---|---|---|---|---|---|---|---|---|
| $\alpha$ | 9.66 | 17.20 | 8.32 | 65 | 20.29 | 78.83 | 23.60 | 23.76 | 37.49 | 7 |
| $\alpha$ | 9.45 | 17.08 | 8.02 | 68 | 20.27 | 78.39 | 23.94 | 24.94 | 37.12 | 8 |
| $\alpha$ | 9.56 | 17.25 | 8.01 | 67.5 | 20.11 | 77.74 | 24.05 | 24.78 | 37.21 | 9 |
| $\alpha$ | 9.65 | 17.20 | 8.11 | 66.3 | 20.10 | 77.74 | 23.97 | 24.34 | 37.34 | 10 |
| $\gamma$ | 9.62 | 16.6 | 9.35 | 60 | 21.33 | 81.12 | 21.96 | 21.65 | 37.96 | 11 |
| $\gamma$ | 9.56 | 16.9 | 9.33 | 59 | 21.69 | 79.39 | 22.23 | 21.63 | 38.73 | 12 |
| $\gamma$ | 9.68 | 16.68 | 9.14 | 59 | 21.42 | 80.65 | 22.70 | 21.75 | 38.91 | 13 |
| $\alpha$ | 9.42 | 17.26 | 8.25 | 69 | 20.21 | 77.42 | 23.09 | 24.36 | 37.36 | *a* |

[a] Present work.

oriented nylon 6 was found to be 97.5 Å according to the Bragg law. It should be added that when the x-ray beam was incident on the textured sample from the FD, no particular SAXS pattern appeared.

When the X-ray beam was incident on the oriented samples from the direction parallel to CD, the SAXS pattern was in the form of two elongated maxima spread out horizontally as shown in Figure 10b. Such a SAXS pattern has been interpreted in very different ways by different investigators. One of the earlier suggestions for the spread out nature of the maxima in the horizontal direction was that the broadening was due to a small crystallite size in the lateral dimensions of the lamellar crystals.[55-58] But a recent study comparing TEM measurement with a semiquantitative estimate showed that broadening alone could not result in such a large spread of maxima in the horizontal direction.[59] The spread of maxima in the horizontal direction in Figure 10b is best interpreted as a continuously varied set of coupled orientations and thicknesses of lamellae,[59] induced by crystallographic shear in the chain direction of lamellae of initially constant thickness. As determined by the pole figure measurements, the macromolecular chains are aligned in the FD of channel-die. At a very large compression in the LD the channel flow conditions apparently result in sheared, corrugated lamellar crystals. Note that such a shape has apparently formed not by bending or local rotation of the crystals but by simple shearing of the crystals in the chain direction. As a result of such shearing, the thickness of the lamellae in the direction normal to the lamellar surface decreases to $D \cos(\psi)$ as the surface normal tilts by an angle $\psi$ with respect to the chain direction, while the distance in the FD is maintained constant at a level $D$ if the crystalline stem length is assumed not to change during the shearing process. The corrugated shape and the decrease of the lamellar thickness in the normal direction together lead to the broad maxima in the horizontal direction. If the thickness in the normal direction had remained constant due to rigid lamellar rotation, the SAXS pattern should have a circular arc type pattern, which it, clearly, does not have.

In summary, the X-ray studies indicate that the nylon 6, deformed by plane-strain compression in the channel-die to a compression ratio between 3.8 and 4.0, is highly textured in both crystal lattices and lamellar aggregation. The WAXS results show that the crystals are predominantly in the $\alpha$ form. The resultant lattice texture, determined by WAXS, has the following features: (1) the molecular chains are aligned in the flow direction; (2) the (002) planes are perpendicular to the loading direction; and (3) the (200) planes are statistically-equally divided and oriented with their normals in the directions of ±21° away from the constraint direction of the channel-die. These features are illustrated in Figure 11 and indicate

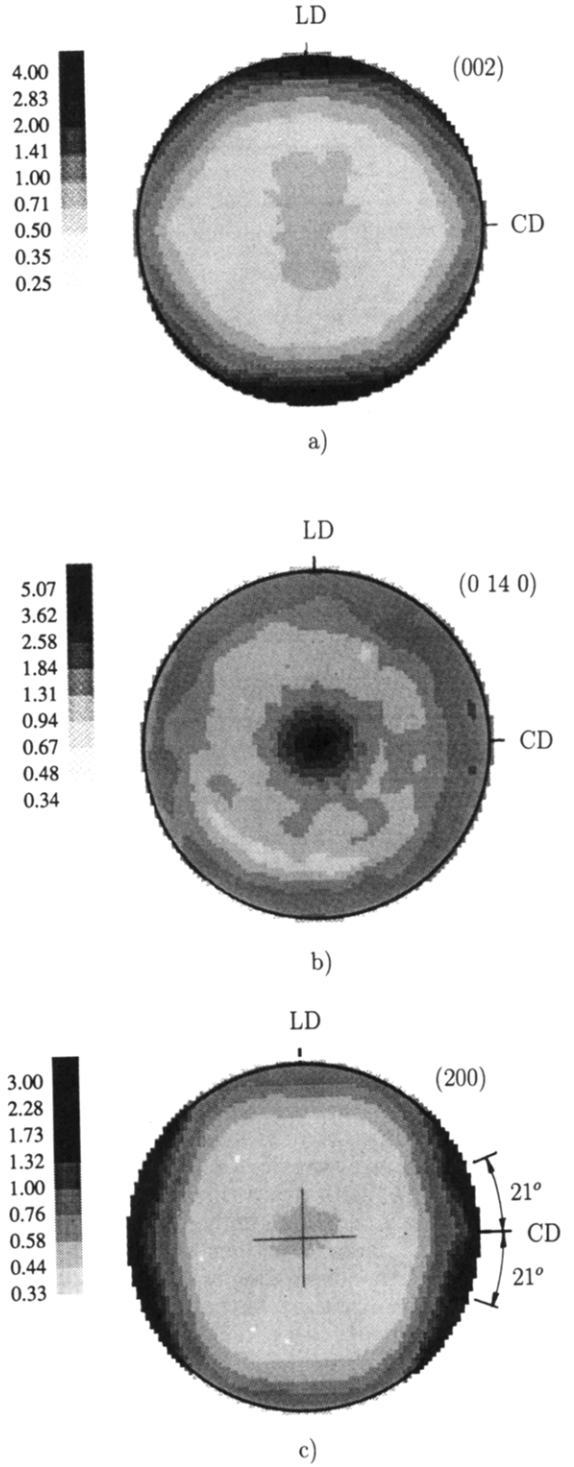


**Figure 9.** Pole figures of textured nylon 6: (a) $2\theta$ = 23.09° for (002) plane diffraction; (b) $2\theta$ = 77.42° for (0 14 0) plane diffraction; (c) $2\theta$ = 20.21° for (200) plane diffraction.

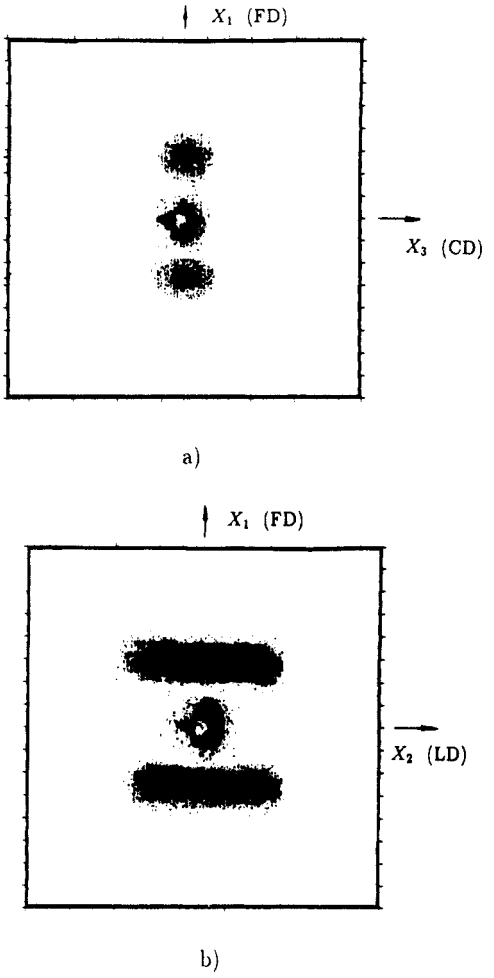


**Figure 10.** Patterns of small-angle X-ray scattering from textured nylon 6: (a) X-ray beam parallel to the $X_2$ direction; (b) X-ray beam parallel to the $X_3$ direction.

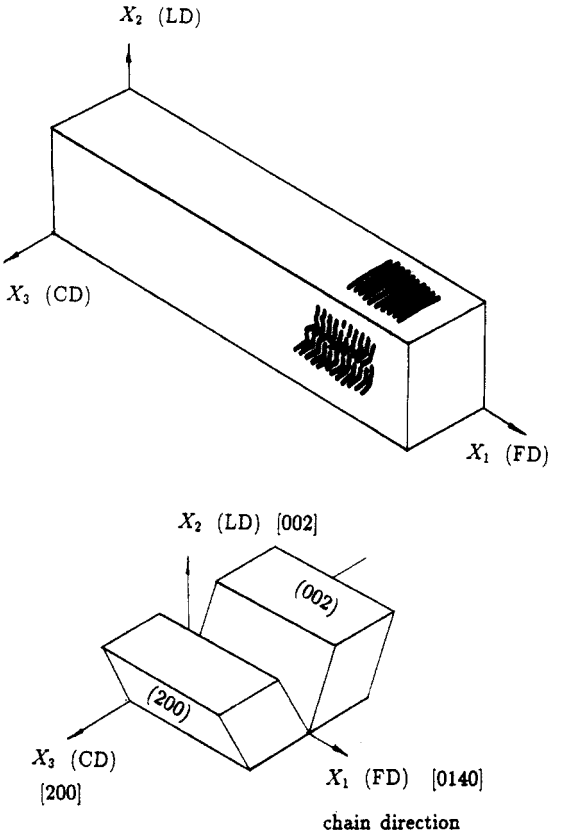


**Figure 11.** Schematic representation of the lattice and lamella orientations of textured nylon 6.

that there is an equal partitioning of monoclinic lamellae between two possible orientations as is shown in the figure. According to the SAXS patterns, the lamellae in the oriented material are "corrugated" in form and can be described by the following: (1) the generator axes of the corrugations are perpendicular to the free flow direction; (2) the edges appear to be straight if they are viewed from the loading direction; (3) the edges appear to be S (or arc) shaped with continuously-varied lamellar thickness, if viewed from the constraint direction. This also illustrated in Figure 11.

Unlike polyethylene, it is impossible to obtain the most desired, so-called, quasi-single-crystal-textured material for nylon 6 by a mechanical process. Due to the nature of the monoclinic structure of nylon 6, the best material that can be obtained for mechanistic studies is the crystallographically dual-oriented material of orthotropic symmetry. The final dimensions of the textured material resulting from the plane-strain compression are 75 mm long, 10 mm wide, and 15 mm high. The relatively large dimensions in all three directions of the well-textured samples provide great advantages for the elastic and plastic anisotropy studies discussed in the following sections.

**3.2. Elastic Anisotropy of Textured Nylon 6.** The experimental measurements of the set of nine elastic compliances of the highly textured orthotropic nylon 6 are listed in column 1 of Table IV. They are the average values from eight measurements with maximum deviations smaller than 15%. The reference coordinates are the three principal axes of the textured material. The elastic constants found from experimental and theoretical studies

**Table IV**
**Elastic Compliances of Nylon 6 ($GPa^{-1}$)**

| | | | | |
|---|---|---|---|---|
| $S_{11}$ | 0.163 | 0.365 | 0.120 | 0.0032 |
| $S_{22}$ | 0.281 | | | 0.3838 |
| $S_{33}$ | 0.232 | 0.260 | 0.212 | 0.1234 |
| $S_{12}$ | −0.105 | | | −0.0010 |
| $S_{13}$ | −0.066 | −0.225 | −0.046 | −0.0001 |
| $S_{23}$ | −0.124 | | −0.106 | −0.1203 |
| $S_{44}$ | 0.970 | 0.6 | | 0.4103 |
| $S_{55}$ | 0.720 | 1.9 | | 1.1731 |
| $S_{66}$ | 1.956 | 3.09 | | 0.4195 |
| ref | [a] | 18 | 60 | 61 |

[a] Present work.

by other investigators are also listed in the table for comparison with the present work. Columns 2 and 3 contain the experimental measurements of textured nylon 6 by Lewis and Ward[18] and Leung et al.[60] Column 4 contains theoretical predictions for $\alpha$-form crystals of nylon 6, by Tashiro and Tadakoro.[61] These values are not those appearing in the original publication, since coordinate axis rearrangement and rotation[62] were necessary in order to relate them properly to the measurements of the orthotropic material of the present work.

In comparison, our measurements are generally smaller than those of Lewis and Ward[18] but larger than those of Leung et al.[60] Among these three groups of measurements, our data agree best with those of Leung et al. Of all the compliances $S_{33}$ shows the best agreement among these three groups. It can be seen from Table IV that some experimental measurements of textured materials are quite close to the theoretical calculation of the elastic constants of the crystals, for example, the compliances $S_{22}$ and $S_{33}$. However, some other measurements differ from the theoretical predictions by as much as 2 orders of magnitude; for example, the compliances $S_{11}$, $S_{12}$, and $S_{13}$. This agreement or the lack of it should be explainable by the structural and morphological characteristics of the highly textured material as discussed above.

From Table IV, we note that the largest differences in the compliances between the experimental measurements of highly textured nylon 6 and theoretical predictions are associated with the $X_1$ direction. We recall from the above section that, in the highly textured nylon 6, lamellar crystals, separated by amorphous layers with overall long-period spacings less than 100 Å, were arranged in series in the $X_1$ direction. It is logical to approximate that the microscopic strains $\epsilon_{11}^c$ from the crystalline component and strains $\epsilon_{11}^a$ from the amorphous component are additive in the $X_1$ direction to make up the overall macroscopic strain $\epsilon_{11}$ and that the stresses $\sigma_{11}^c$ and $\sigma_{11}^a$ acting through both the components are the same as the applied stress $\sigma_{11}$ to satisfy the equilibrium condition. Thus, as an upper bound, the total compliance $S_{11}$ of the textured material is a summation of the weighted compliances $S_{11}^c$ and $S_{11}^a$ of the two components. Since the crystallinity of nylon 6 used in the present work is 43.4%, the contributions from these two component compliances to the total compliance should be about equally weighted. Furthermore, since the elastic compliance $S_{11}^c$ of the crystals in the chain ($X_1$) direction is smaller than the elastic compliance $S_{11}^a$ of the amorphous component by order(s) of magnitude due to the continuous covalent bonds in the same direction, the compliance $S_{11}$ of the highly textured two-component material is governed by the compliance $S_{11}^a$ of the amorphous component. Therefore, there should not be much connection between $S_{11}$ and $S_{11}^c$.

In the $X_2$ and $X_3$ directions, however, the situations are very different from that in the $X_1$ direction. First, in these directions, the material is better approximated by a parallel arrangement of the crystalline and amorphous components. The strains $\epsilon_{22}^c$ and $\epsilon_{22}^a$ of the two components should be the same as the macroscopic strain $\epsilon_{22}$ of the textured material, and the $\epsilon_{33}^c$ and $\epsilon_{33}^a$ should be the same as the $\epsilon_{33}$, in order to satisfy compatibility in these two directions. The reciprocals of lower bounds of the total compliances $S_{22}$ and $S_{33}$ of the textured material are summations of corresponding weighted reciprocals of compliances of the two components. Second, it is reasonable to assume that the compliances $S_{22}^c$, $S_{33}^c$, $S_{22}^a$, and $S_{33}^a$ are of the same order of magnitude, since molecular chains interact through van der Waals forces and hydrogen bounds in transverse directions. Thus, the total compliances $S_{22}$ and $S_{33}$ should be in the same order of magnitude as the compliances of its components and appear to have obvious connections to the corresponding compliances of the crystalline component.

The morphological features in these two directions make it possible to relate directly the overall compliances $S_{22}$ and $S_{33}$ of the textured material to the compliances $S_{22}^c$ and $S_{33}^c$ of the lamellar crystals. Furthermore, the morphological similarity in these two directions allows us to directly compare the compliances $S_{22}$ and $S_{33}$. From Table IV, it can be seen that the theoretical prediction of $S_{33}^c$ is smaller than that of $S_{22}^c$ and that the measurement of $S_{33}$ is smaller than that of $S_{22}$. The difference in the crystalline compliances can be attributed to the existence of hydrogen bonds in the $X_3$ direction, which are several times stronger than van der Waals interactions holding molecular chains together in transverse directions. This difference directly manifests itself in the overall compliances of the textured samples.

The shear compliances in Table IV indicate substantial disagreements between the groups. On the crystallographic scale, the resolved shear stress $\sigma_{23}$ must overcome van der Waals interactions to result in sliding on (002) planes or to overcome van der Waals interactions plus hydrogen bonds to result in sliding on (200) planes. The stress $\sigma_{13}$ must overcome covalent bonds to result in sliding on (0 14 0) planes or van der Waals interactions plus hydrogen bonds to result in sliding on (200) planes. Similarly, the stress $\sigma_{12}$ must overcome van der Waals interactions or covalent bonds. Since a weaker interaction or bond allows a larger displacement (strain), the shear compliances of crystals are governed by the corresponding weaker ones of each pair of the forces. This qualitative argument leads to the conclusion that the compliance $S_{44}^c$ ($S_{2323}^c$) should be larger than the compliance $S_{55}^c$ ($S_{1313}^c$), the $S_{66}^c$ ($S_{1212}^c$) larger than the $S_{55}^c$, and the $S_{44}^c$ approximately equal to the $S_{66}^c$. On a larger scale, the morphology of the textured material suggests that both the strain $\epsilon_{23}^c$ of the crystalline component and the strain $\epsilon_{23}^a$ of the amorphous component should be the same as the macroscopic strain $\epsilon_{23}$ of the textured sample. Thus, the measured value of $S_{44}$ should approach the lower bound estimate on the compliance. However, no simple comparison can be made between the $S_{44}$ and the other two shear compliances because of the differences in morphology and in the crystalline compliances. Since there is a morphological similarity for the compliances $S_{55}$ and $S_{66}$, the lower value of $S_{55}$ in comparison to $S_{66}$ can be attributed to the effect of hydrogen bonding in the crystallites.

A better interpretation of the experimental results and their deconvolution into a unique set of measurements attributable to the crystalline and amorphous components requires model calculations. Such calculations are now in progress and will be reported separately in the future elsewhere.

**3.3. Plastic Deformation Mechanisms.** Usually, elastic resistance and inelastic resistance of a material are closely related, since the latter often relates to elastic strain energy storing shear transformation. The deformation of highly textured nylon 6 exhibits certain important characteristics that must be noted.[63] While the elastic shear modulus in the longitudinal shear direction parallel to the chain axis of the highly textured material undergoes a very significant drop around 310 K due to an apparent glass transition in the amorphous component, there is no related discontinuity in the critical resolves shear stress with temperature change in this range. This indicates that at the initial yield the plastic deformation resistance primarily results from the crystalline component of the material.

At moderate strains, the plastic deformation occurring in nylon 6 crystals is crystallographic in nature. This is suggested by the X-ray results of the highly textured materials. The above results show that even after a plastic strain as large as 150% (compression ratio 4), the crystalline order of the nylon 6 crystals was still maintained, although the texture of the material was changed very substantially, from an initial isotropic random orientation to a quasi-single crystal texture. In fact, the crystallinity of the material even increased slightly after the deformation (Table II). To maintain the crystalline order of a material during plastic deformation, the deformation of crystallites must be in a very orderly form of crystallographic slip.

The long-chain nature of polymer molecules, which makes them relatively inextensional in the chain direction, requires that the most preferred slip plane in polymer crystals contains the molecular chain, since the covalent bonds in the chain backbone are much stronger than those of the van der Waals interactions and hydrogen bonds

acting in the transverse directions of molecular chains for holding the neighboring chains together. The molecular chains can remain unbroken through indefinitely large shear translations parallel to the chain axis.[64,65] This means that the crystallographic deformation plane must be of the (*h*0*l*) type for nylon 6 crystals until a very large plastic strain is reached that effectively shears the crystallites apart. Furthermore, the character of the nylon 6 crystal structure suggests that the two most likely slip planes are the crystallographic (002) and (200) planes (Figure 1a), since they are the two most closely packed planes with the largest interplanar distances in the crystal lattice, which should give the lowest shear resistance.

For the (002) slip plane, the slip direction should be of the [*vu*0] type. The most likely slip directions are [010] and [100], since the Burgers vectors in these two directions are the shortest. Here the Burgers vector for the [010] slip is taken to be $^1/_7$ of the lattice parameter *b* since shear in this direction occurs, most likely, by partial dislocation motion. These two independent slip systems, (001)[010] and (001)[100], can result in a shear strain in any direction on the (001) plane. For the same reason, the slip direction should be of the [0*uw*] type, and the most preferred slip directions, therefore, are [010] and [001] for the (100) slip plane. But the (100)[001] transverse slip system may be difficult to activate in the textured nylon 6 obtained from plane-strain compression, since there are two possible orientations of the [001] crystallographic direction due to the nature of the monoclinic crystals. Slip in one of the [001] directions is restricted by the complementary crystals which have their [001] direction in another direction. In summary, the deformation modes that are most probable to become active in nylon 6 are (001)[010], (100)[010], and (001)[100] slip systems.

One form of evidence for the presence of a specific deformation mode is the appearance of shear bands and the change of shape of deformed samples. Figures 5 and 6 show some examples of the deformed samples. Since the three crystalline deformation modes result in shear in planes perpendicular to the amorphous layers, the competing "interlamellar shear" of the amorphous component, if it occurred, can be easily distinguished by examining the orientations of the shear bands and the shape of the deformed samples. The orientations of the shear bands and the shape of the deformed samples that are shown in Figures 5 and 6 indicate that the plastic deformation occurred by crystalline shear.

The final texture (Figure 9) resulting from the plane-strain compression process indicates that the principal slip plane which usually orients itself normal to the principal compression direction is the (001) plane and that the principal direction of slip in this slip plane which usually aligns itself parallel to the principal direction of extension is the [010] chain direction. In other words, the (001)[010] slip system is the predominant deformation mode of nylon 6. During plane-strain compression of nylon 6, the (001)[010] chain slip mechanism was first activated and continued to play the dominant role in the whole process. The activity of the (001)[010] slip system produces rotation of chain axes about the *a*-axis toward the principal plastic flow direction. The rotation continues monotonically as the plastic deformation continues. At about a compression ratio of 4.0, the orientations of molecular chains were changed from complete randomness to almost complete alignment in the flow direction, and the (001) plane normals were changed to be nearly parallel to the compression direction, as clearly indicated by the pole figures of Figure 9. It should be noticed that transverse slip on the (001) plane, i.e., the (001)[100] slip, is also necessary for the rotation of the (001) plane normals toward the compression direction, although a relatively large stress may be required to activate this deformation system.

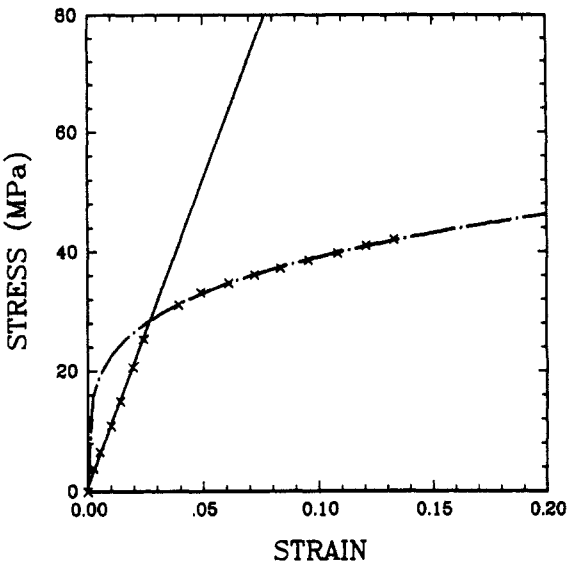


**Figure 12.** Typical stress–strain data obtained from digitization of an experimental curve for determination of the yield point.

**3.4. Anisotropic Plastic Resistances of Textured Nylon 6.** Figure 12 shows a set of stress–strain data of uniaxial tension of the oriented nylon 6. Before the sample was deformed, the angle between the loading direction and the slip direction of the sample was 45°. This experiment was to activate the (001)[010] slip system. But this set of stress–strain data is quite representative for all the experiments in determining the yield behavior of the textured material. From this figure, it can be seen that, at the early portion of the curve, the slope is constant, representing an elastic response of the material. Then the slope decreases gradually with increasing strain as a transition from elastic to plastic response occurs. After the transition is complete, the slope continues to decrease, albeit slowly. Since both stress and strain vary smoothly during the transition, the exact yield point is not easy to determine. Therefore, the yield point was defined by adopting a special construction, as illustrated in Figure 12. For each stress–strain curve, the very early portion of the curve was fitted to a straight line relation, and the well-developed plastic portion was fitted to a power law relation approaching zero strain with infinite slope. The intersection of the straight line and the parabola was taken as the yield point.

The yield stress as a function of the angle $\phi_0$ for activating the three principal deformation systems is plotted in Figure 13. For the deformation systems (001)[010] and (100)-[010] resulting in chain slip, the yield results were obtained from both compression and tension experiments. In the figure, the solid data points refer to the tension and the open points to the compression results. For the (001)-[100] system resulting in transverse slip, only the compression experiments were successful. The tensile samples for this slip system always fractured before any observable yield behavior was reached, and the fractures always occurred on the (001) planes and along the [100] crystallographic direction regardless of the initial orientation of the [100] slip direction. This suggests the presence of some structural weakening initiating the fracture in the transverse direction to the molecular chains. The Burg-

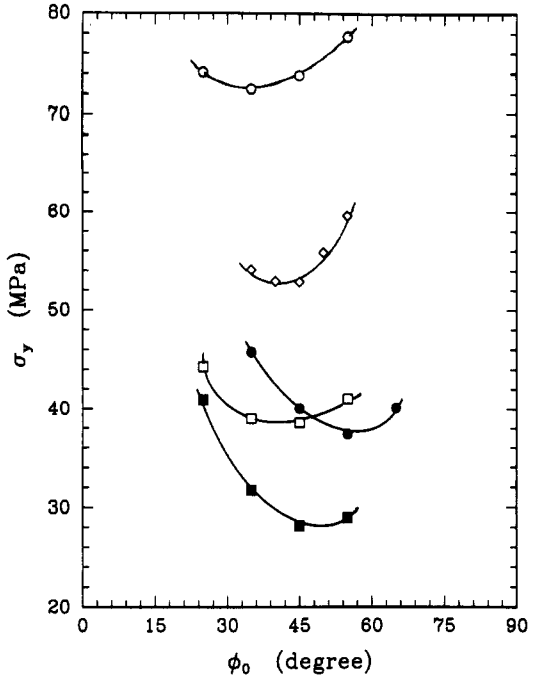


**Figure 13.** Plots of initial yield stress vs initial angle $\phi_0$ for the (001)[010] slip (□,■), the (100)[010] slip (○,●), and the (001)-[100] slip (◇). Open data points are from compression experiments and solid data points from tension experiments.

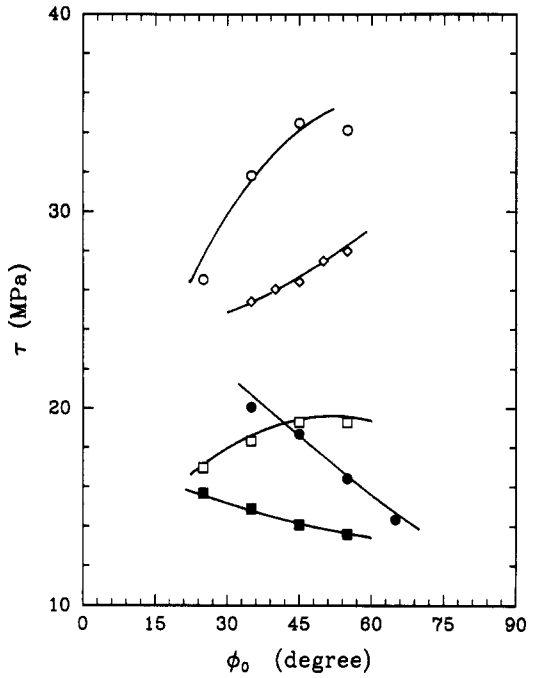


**Figure 14.** Plots of resolved shear stress vs initial angle $\phi_0$ for the (001)[010] slip (□,■), the (100)[010] slip (○,●), and the (001)-[100] slip (◇). Open data points from compression experiments and solid data points from tension experiments.

ers vector of a dislocation responsible for the (001)[100] transverse slip should be 9.42 Å, which is quite large in comparison to 2.46 Å for chain slip. This means that a molecular segment has to translate a large distance in order to reregister into a similar neighborhood. Large Burgers displacements mean larger dislocation line energies and larger slip resistances. Thus, if the characteristic strength impairing flaws are likely to propagate before slip can be initiated, premature fracture will result. This is believed to be the case when shearing the textured nylon 6 in the [100] transverse direction in tension. Apparently, in compression where the flaws are likely to be pressed together, slip occurs before the flaws can result in fracture.

Figure 13 indicates that the textured nylon 6 is plastically highly anisotropic. Not only are the slip resistances very different when deforming the material on different slip systems but also, for the same slip systems, the shear resistances under compression are very different from those under tension. The initial yield stress $\sigma_y$ varies from 28.17 to 77.76 MPa in the limited experimental range of the angle $\phi$. The anisotropy is caused by the crystal texture of the material and the differences in plastic deformation resistance for different deformation systems.

For the (001) plane deformation systems, the resolved shear stress $\tau$ acting on the slip plane at their initial yield is

$$\tau = \sigma_y \sin \phi_y \cos \phi_y \tag{7}$$

and the corresponding normal stress acting on the slip plane is

$$\sigma_n = \sigma_y \sin^2 \phi_y \tag{8}$$

where $\phi_y$ is the angle between the direction of the applied stress and the slip direction at the initiation of slip on the systems. For the (100) plane deformation system, the resolved shear stress $\tau$ is given by

$$\tau = \sigma_y \sin \phi_y \cos \phi_y \sin \beta \tag{9}$$

and

$$\sigma_n = \sigma_y \sin^2 \phi_y \sin^2 \beta \tag{10}$$

where the extra terms involving the crystallographic angle $\beta$ are necessary to account for the tilt of the (100) plane normal away from the $X_3$ direction by the angle $(90 - \beta)$. Since there are two different orientations of the (100) planes in the highly textured orthotropic nylon 6, as described in section 3.3, it is impossible to shear one type of (100) plane without also shearing the other type of (100) plane. In the experiments as described above, shear stress and normal stress were applied on the $X_1X_2$ plane in the channel-die coordinates, which bisects the two different (100) planes. Although there is no clear evidence for (100) plant slip, the assumption that slip should be on the (100)-[010] slip system is reasonable because, in the most competitive orientations, the two types of (100) plane are the most closely packed planes and have the largest interplanar distance. They are also the planes with the highest Schmid factor in this type of stressing.

The angle $\phi$ between the direction of the applied stress and the slip direction of a slip system that is being activated is not constant during deformation. The changes in angle from $\phi_0$ at zero stress to $\phi_y$ at initial yield were estimated through an elastic deformation analysis without considering the morphological details of the material, which is described elsewhere.[62] The analysis indicates that the maximum change is approximately 3° and that the effects of slip-direction rotation on the accuracy of establishing the yield condition is very small. In the following, the angle $\phi_y$ will be approximated by the initial angle $\phi_0$.

Figure 14 summarizes the resolved shear stresses required to initiate slip on the three principal deformation systems. It shows that the shear resistances of each individual deformation mode do not approach single values. Therefore, the Schmid law of resolved shear stress, which states that plastic deformation occurs on the crystallographic slip system when the resolved shear stress in a special slip direction reaches a critical value, is not an adequate description for the nylon 6 crystals and requires further consideration.

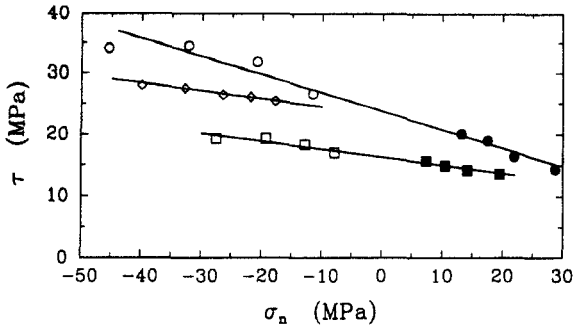


**Figure 15.** Yield conditions of the (001)[010] slip (□,■), the (100)[010] slip (○,●), and the (001)[100] slip (◇). Open data points are from compression experiments and solid data points from tension experiments.

**Table V**
**Critical Resolved Shear Stresses and Normal-Stress Sensitivity Factors**

| slip system | $\tau_0$ (MPa) | $\mu_0$ |
|---|---|---|
| (001)[010] | 16.24 | 0.13 |
| (100)[010] | 23.23 | 0.28 |
| (001)[100] | 23.18 | 0.13 |

The measured plastic yield conditions for the three deformation systems are summarized in Figure 15. The positive normal stresses resulted from the tension experiments, while the negative normal stresses resulted from the compression experiments. This figure clearly indicates that the shear resistance for plastic deformation depends on normal stress acting on the shear planes. Furthermore, this behavior can be approximated by a linear relation of the type

$$\tau = \tau_0 - \mu_0 \sigma_n \tag{11}$$

where $\tau_0$ is called the critical resolved shear stress (CRSS) in the absence of any normal stress on the slip planes and $\mu_0$ is called the normal stress sensitivity factor (NSSF). The above relation is known as the Coulomb yield criterion,[67] that is found to be widely applicable to granular materials. This criterion is, however, rarely used in the plasticity of metal crystals since the pressure dependence of the yield is not prevalent for metallic materials at the usually relatively low levels of CRSS of these materials in comparison to their shear moduli. But for semicrystalline polymers, as in other polymers where the plastic resistance is a substantial fraction of the shear modulus, the normal stress (or pressure) dependence of yield is substantial. Several groups of investigators[23,68-70] found that the stress required to shear oriented polyethylene in the chain directions is a linear function of the normal stress imposed on the shear plane. The normal stress dependence of the shear resistance was also reported for amorphous polymers.[71-73] The present experimental data strongly suggest that the dependence of the shear resistance on the normal stress is well represented as a linear relation. Thus, a modification of the Schmid law based on the Coulomb criterion describes the yield behavior of polymers, phenomenologically, as

$$\sigma_y = \frac{\tau_0}{\sin\phi\cos\phi + \mu_0 \sin^2\phi} \tag{12}$$

By fitting this relation to the experimental data, the CRSS $\tau_0$ and NSSF $\mu_0$ were determined for the three principal deformation mechanisms of nylon 6 crystals and are summarized in Table V.

In comparison with the two (001) plane slip systems, the yield condition shifts upward when slip occurs in the transverse direction. In other words, slip in the chain direction is easier to be activated than in the transverse direction. This is consistent with the finding of the resultant texture of the plane-strain compression samples. Otherwise, the [100] crystallographic direction should have been parallel to the flow direction of the channel-die. The reason for the low shear resistances of the (001)[010] chain slip system is that dislocations for chain slip have Burgers vectors much smaller than dislocations for the (001)[100] transverse slip system.

In comparison of the two chain slip systems, the shear resistance of the (100)[010] system is found to be higher and the effect of normal stress on the shear resistance is greater than that of the (001)[010] chain slip system. From the crystal structure point of view, there are several factors that may cause this difference: the distance between crystallographic slip planes, the orientation of the planes in which the zigzags of the molecules are confined, the orientation of the planes of chain folding, and existence of the hydrogen bonds between chains. For nylon 6 $\alpha$ crystals, the (200) interplanar distance $d_{200}$ is 4.4 Å, and (002) is 3.85 Å; the zigzag planes and the folding planes are either known to be or can be taken to be parallel to the (002) plane; and hydrogen bonds are situated in the transverse direction similar to the van der Waals forces but are in the (002) planes. In one crystal unit cell, there are 14 pairs of van der Waals interactions in the (200) planes. In comparison, there are 12 pairs of van der Waals forces and 2 pairs of hydrogen bonds in the (002) planes. Generally the hydrogen bond is several times stronger than the van der Waals interaction and should have more profound effects.

The interplanar distance can play a dominant role in determining the shear resistance of a material based on fundamental considerations of dislocation mobility on such planes. Usually, the larger the interplanar distance of a deformation system, the lower the shear stress required to initiate the slip activity. Young et al.[23] found that the shear resistance is approximately inversely proportional to the interplanar distance, where, e.g., the CRSS for the (100)[001] and (010)[001] slip systems of polyethylene were 10 and 15 MPa, respectively. The corresponding interplanar distances are 7.4 and 4.93 Å for those two planes. The ratio of the critical resolved shear stress to be reciprocal of the interplanar distance can be calculated to be a value 74 for both the (100)[001] and (010)[001] slip systems in that crystal structure. Although it may be accidental that the exact same value was found for these two systems, it does show a consistent trend. For nylon 6 crystals, the interplanar distance of (001) planes is smaller than that of (100) planes. If there was no criterion other than that just discussed, the (001)[010] slip should be more difficult to be activated than the (100)[010] slip. But the experimental results show that the shear resistance of the (001)[010] slip is much lower than that of the (100)-[010] slip. Therefore, one or more of the other three structural features in the nylon 6 crystals must play the dominant role. The highly textured nylon 6 contains principally the $\alpha$ form of crystals. Since hydrogen bonds in $\alpha$ crystals lie in the (001) planes, permanent sliding on the (001) planes will not break the hydrogen bonds, but sliding on the (100) planes will do so. If there were no hydrogen bonds, the zigzag configuration of molecules out of the (100) planes, and constraints arising from the character of molecular folding, the shear resistance of the (100)[010] slip would be 14.22 MPa, corresponding to 16.24 MPa of the (001)[010] slip. In this estimate, it is assumed, crudely, that the shear resistance of a slip system is linearly

proportional to the reciprocal of the interplanar distance of the shear planes. Replacing two pairs of the van der Waals forces by two pairs of hydrogen bonds and the addition of the out-of-slip-plane zigzag shape and the folding character of the molecules should lead to an increase in shear resistance by about 9 MPa, corresponding to a total resistance of 23.22 MPa for the (100)[010] slip when no normal stress is acting across the (100) slip planes. The out-of-plane structural features make the (100)[010] slip require a larger shear stress than the (001)-[010] slip.

Figure 15 shows that the normal stress dependences of the shear resistances are almost identical for the two slip systems associated with the (001) crystallographic plane. Since the principal difference between these two slip systems is the Burgers vectors in both magnitude and direction, it must be concluded that the effect of normal stress has little to do with the Burgers vector of the deformation system.

The NSSFs $\mu_0$ obtained (Table V) indicate that the normal stress dependence of the shear resistance for slip on (100) planes is more than twice as high as that for slip on (001) planes. Part of this can be attributed to the existence of hydrogen bonds in nylon 6 crystals, since the hydrogen bonds have to be overcome for molecules to slide on (100) planes, and the resistance of hydrogen bonds may be dependent on the normal stress. Another reason for the higher normal stress dependence of the shear resistance of the (100)[010] slip system is that the zigzag planes of molecular chains are formed in the (001) planes. The C–H, N–H, and C=O groups make the (100) planes much "rougher" on the molecular scale than the (001) planes in nylon 6. The factor $\mu_0$ of the normal-stress dependence of shear resistance increases by an amount of 0.15 through the hydrogen bonds and the molecular zigzag shape out of the slip planes. The combination of the long-chain nature of molecules making up polymers and the relatively large size of the unit cells of polymer crystals must be responsible for the difference of their yield behavior in comparison with metal crystals. This is supported by the fact that the out-of-plane N–H and C=O groups increase the roughness of slip planes and result in larger normal-stress dependence of the (100)[010] slip than the (001)-[010] slip. The critical resolved shear stresses are usually a much larger fraction of the elastic moduli in polymers than they are in metals. This is another reason for the high sensitivity to normal stress of polymers, as the increased normal compression stresses increase the elastic stiffness of the material which in turn scales the plastic resistance. Clearly, the above discussion relating the slip resistances to interplanar spacing and whether or not hydrogen bonds are to be negotiated over are of a phenomenological nature but must reflect more fundamental underlying mechanisms governing dislocation mobility in these slip systems that need to be explored from more basic considerations.

In comparison with polyethylene, nylon 6 has a more complicated crystal structure but fewer apparent deformation modes. The predominant deformation mechanism is crystallographic slip for both materials in semicrystalline form. Mechanical twinning and stress-induced martensitic phase transformations are known to occur to some degree in the deformation of polyethylene. No corresponding twinning or martensitic transformations were detected in the deformation of either textured or untextured nylon 6 in the present work or in deformation studies of single crystals on Mylar substrates at room temperature.[74] The shear resistances associated with each deformation mode of nylon 6 are higher than those of the corresponding modes of polyethylene. The differences must be not only due to the different structures but also due to the existence of hydrogen bonds in nylon 6. On the macroscopic scale, the yield strength of isotropic nylon 6 is also higher than that of isotropic polyethylene.[75] These macroscopic behavior characteristics directly relate to the shear resistances of individual deformation modes on the microscopic scale. Clearly, in this difference of behavior there can also be an indirect role played by the amorphous material which has quite different $T_g$ for these two materials.

## IV. Conclusions

In the present study we have demonstrated that samples of substantial size of nylon 6 with dual lattice orientations in overall orthotropic symmetry and with simpler and well-defined lamellar morphology in near quasi-crystal perfection can be produced by plane-strain compression in a deep channel-die. The predominant deformation mode resulting in the material texture in this process is the (001)-[010] crystallographic slip system. The dominant crystalline state of the oriented material is in $\alpha$ form. The resultant lattice texture determined by WAXS is that molecular chains are aligned in the flow direction, the (010) and (001) plane normals are parallel to the flow direction and the loading direction, respectively, and the (100) plane normals make angles of $\pm 21°$ with the constraint direction of the channel-die, indicating the existence of a dual morphology of crystallites in the textured end product. The lamellae in the oriented materials are revealed by SAXS patterns, as S-shaped corrugated sheets with their straight generator lines lying parallel to the constraint direction but having a constant thickness in the flow direction, resulting apparently by shear of sheets parallel to the chain direction. The relatively large dimensions of the textured material, which to a first approximation is in single crystalline form, make it possible to study the crystal plasticity characteristics.

The textured nylon 6 is highly anisotropic. A complete set of nine elastic compliances of the material has been determined by direct mechanical experiments. While the present work is not the first that has measured elastic constants of highly textured polymers, it is the first that has obtained all constants with a single technique. The simplicity of the present technique makes it possible for the first time to study in a more complete manner elastic behavior under other experimental conditions of, e.g., pressure and temperature.

The principal plastic-deformation modes in lamellar crystals of nylon 6 are (001)[010], (100)[010], and (001)-[100] crystallographic slip. Among these, the (001)[010] chain slip is the easiest one to be activated. The yield conditions associated with each of these three deformation mechanisms indicate that the resolved shear stresses required to initiate slip increase linearly with the normal compressive stress acting on the corresponding slip planes. Therefore, the yield behavior of the lamellar crystals can be characterized by the critical resolved shear stress and normal-stress sensitivity factor for each deformation mode. At room temperature, these are 16.2 MPa and 0.13 for the (001)[010] chain slip, 23.1 MPa and 0.13 for the (001)-[100] transverse slip, and 23.2 MPa and 0.28 for the (100)-[010] chain slip. Comparisons of the yield conditions between these three deformation modes indicate that hydrogen bonds existing in nylon 6 crystals play an important role in governing in the slip resistances. When they lie in the slip plane, as in the (001)[010] system, the

hydrogen bonds are not broken by interplanar shear. When they bridge across the slip plane, as in the (100)[010] system, they significantly raise the slip resistance.

## References and Notes


(1) Ward, I. M., Ed. *Structure and Properties of Oriented Polymers*; Halsted Press–Wiley: New York, 1975.
(2) Ciferri, A., Ward, I. M., Eds. *Ultra-High Modulus Polymers*; Applied Science Publishers: London, 1979.
(3) Asaro, J. R. *Advances in Applied Mechanics*; Academic Press: New York, 1983; Vol. 23, p 1.
(4) Ahzi, S.; Argon, A. S.; Bartczak, Z.; Parks, D. M., to be published in *Macromolecules*.
(5) Young, R. J.; Bowden, P. B. *J. Mater. Sci.* **1973**, *8*, 1177.
(6) Galeski, A.; Argon, A. S.; Cohen, R. E. *Makromol. Chem.* **1987**, *188*, 1195.
(7) Brill, R. *Z. Phys. Chem.* **1943**, *B-53*, 61.
(8) Wallner, L. G. *Monatsh. Chem.* **1948**, *79*, 279.
(9) Holmes, D. R.; Bunn, C. W.; Smith, D. J. *J. Polym. Sci.* **1955**, *17*, 159.
(10) Ruscher, C.; Schröder, H. J. *Faserforsch. Textiltech.* **1960**, *11*, 165.
(11) Ota, T.; Yoskizaki, O.; Nagai, E. *J. Polym. Sci., Part A* **1964**, *2*, 4865.
(12) Arimoto, H. *J. Polym. Sci., Part A* **1964**, *2*, 2283.
(13) Illers, H. K.; Haberkorn, H.; Simak, P. *Makromol. Chem.* **1972**, *158*, 285.
(14) Parker, J. P.; Lindenmeyer, P. H. *J. Appl. Polym. Sci.* **1977**, *21*, 821.
(15) Hoashi, K.; Andrews, R. D. *J. Polym. Sci., Part C* **1972**, *38*, 389.
(16) Miyasaka, K.; Makishima, K. *J. Polym. Sci., Part A* **1967**, *5*, 3017.
(17) D'Alo, B.; Coppola, G.; Pallesi, B. *Polymer* **1974**, *15*, 130.
(18) Lewis, E. L. V.; Ward, I. M. *J. Macromol. Sci., Phys.* **1980**, *B18*, 1.
(19) Lewis, E. L. V.; Ward, I. M. *J. Macromol. Sci., Phys.* **1981**, *B19*, 75.
(20) Lin, L.; Argon, A. S. *A Review: Structure and Deformation of Polyethylene*; to be published.
(21) Cowking, A.; Rider, J. G. *J. Mater. Sci.* **1969**, *4*, 1051.
(22) Hay, I. L.; Keller, A. *Kolloid Z. Z. Poly.* **1965**, *204*, 43.
(23) Young, R. J.; Bowden, P. B.; Ritchie, J. M.; Rider, J. G. *J. Mater. Sci.* **1973**, *8*, 23.
(24) Burnay, S. G.; Aere, M. D. D.; Groves, G. W. *J. Mater. Sci.* **1978**, *13*, 639.
(25) Frank, F. C.; Keller, A.; O'Connor, A. *Philos. Mag.* **1958**, *3*, 64.
(26) Allan, P.; Bevis, M. *Philos. Mag.* **1980**, *41*, 555.
(27) Geil, P. H. *J. Polym. Sci., Part A* **1964**, *2*, 3818.
(28) Kiho, H.; Peterlin, A.; Geil, P. H. *J. Appl. Phys.* **1964**, *35*, 1599.
(29) Tanaka, K.; Seto, T.; Hara, T. *J. Phys. Soc., Jpn.* **1962**, *17*, 873.
(30) Sakaoku, K.; Peterlin, A. *Makromol. Chem.* **1972**, *157*, 131.
(31) Allan, P.; Crellin, E. B.; Bevis, M. *Philos. Mag.* **1973**, *27*, 127.
(32) Galeski, A.; Argon, A. S.; Cohen, R. E. *Macromolecules* **1988**, *21*, 2761.
(33) Galeski, A.; Argon, A. S.; Cohen, R. E. *Macromolecules* **1991**, *24*, 3945.
(34) Galeski, A.; Argon, A. S.; Cohen, R. E. *Macromolecules* **1991**, *24*, 3953.
(35) Hay, I. L.; Keller, A. *J. Mater. Sci.* **1966**, *1*, 41.
(36) Buckley, C. D.; Gray, R. W.; McGrum, N. G. *J. Polym. Sci., Part B* **1970**, *8*, 341.
(37) Pope, D. P.; Keller, A. *J. Polym. Sci., Polym. Phys. Ed.* **1975**, *13*, 533.
(38) Point, J. J.; Homes, G. A.; Gezovich, D.; Keller, A. *J. Mater. Sci.* **1969**, *4*, 908.
(39) Pope, D. P.; Keller, A. *J. Mater. Sci.* **1974**, *9*, 920.
(40) Wlochwicz, A.; Jezioeny, A. *J. Polym. Sci., Polym. Chem. Ed.* **1974**, *12*, 793.
(41) Vogelsong, D. C. *J. Polym. Sci., Part A* **1963**, *1*, 1055.
(42) Inoue, K.; Hoshino, S. *J. Polym. Sci., Polym. Phys. Ed.* **1977**, *15*, 1363.
(43) Matyi, R. J.; Crist, B. *J. Polym. Sci., Polym. Phys. Ed.* **1978**, *16*, 1329.
(44) Boukal, I. *J. Appl. Polym. Sci.* **1967**, *11*, 1483.
(45) Hadley, D. W.; Pinnock, P. R.; Ward, I. M. *J. Mater. Sci.* **1969**, *4*, 152.
(46) Amuzu, J. K. A. *J. Mater. Sci. Lett.* **1984**, *3*, 291.
(47) Ward, I. M. *Phys. Bull.* **1970**, *21*, 71.
(48) Puffr, R.; Sebenda, J. *J. Polym. Sci., Part C* **1967**, *16*, 79.
(49) Bull, H. B. *J. Am. Chem. Soc.* **1944**, *66*, 1499.
(50) Kapur, S.; Rogers, C. E.; Bear, E. *J. Polym. Sci., Polym. Phys. Ed.* **1972**, *10*, 2297.
(51) Kawasaki, K.; Sekita, Y.; Kanou, K. *J. Colloid Sci.* **1962**, *17*, 865.
(52) Skirrow, G.; Young, K. R. *Polymer* **1974**, *19*, 15.
(53) Christie, M. A.; Darlington, M. W. *Plast. Polym.* **1975**, *43*, 149.
(54) Hunt, D. G.; Darlington, M. W. *Polymer* **1978**, *19*, 977.
(55) Hess, K.; Kiessig, H. *Z. Phys. Chem.* **1944**, *A193*, 196.
(56) Belbeoch, B.; Guinier, A. *Makromol. Chem.* **1955**, *31*, 1.
(57) Bonart, R.; Hosemann, R. *Kolloid Z. Z. Polym.* **1962**, *186*, 16.
(58) Statton, W. O.; Goddard, G. M. *J. Appl. Phys.* **1957**, *28*, 1111.
(59) Song, H. H.; Argon, A. S.; Cohen, R. E. *Macromolecules* **1990**, *23*, 870.
(60) Leung, W. P.; Ho, K. H.; Choy, C. L. *J. Polym. Sci., Polym. Phys. Ed.* **1984**, *22*, 1173.
(61) Tashiro, K.; Tadokoro, H. *Macromolecules* **1981**, *14*, 781.
(62) Lin, L. An Experimental Study of Deformation Mechanisms and Resistances of Semi-Crystalline Polymers. Ph.D Thesis, MIT, 1991.
(63) Lin, L.; Argon, A. S., to be published.
(64) Kausch, H. H. In *Advances in Polymer Science and Engineering*; Pae, K. A., Ed.; Plenum Press: New York, 1972; p 207.
(65) Hammond, C. L.; Hendra, P. J.; Lator, B. G.; Maddams, W. F.; Willis, H. A. *Polymer* **1988**, *29*, 49.
(66) Schmid, E.; Boas, W. *Plasticity of Crystals*; F. A. Hughes & Co. Ltd.: London, 1950; p 105.
(67) Coulomb, C. A. *Mem. Math. Phys.* **1773**, *7*, 343.
(68) Keller, A.; Rider, J. G. *J. Mater. Sci.* **1966**, *1*, 389.
(69) Hinton, T.; Rider, J. G. *J. Appl. Phys.* **1968**, *39*, 4932.
(70) Simpson, L. A.; Hinton, T. *J. Mater. Sci.* **1971**, *6*, 558.
(71) Argon, A. S.; Andrew, R. D.; Godrick, J. A.; Whitney, W. *J. Appl. Phys.* **1968**, *39*, 1899.
(72) Duckett, R. A.; Rabinowitz, S.; Ward, I. M. *J. Mater. Sci.* **1970**, *5*, 909.
(73) Bowden, P. B.; Jukes, J. A. *J. Mater. Sci.* **1972**, *7*, 52.
(74) Geil, P. H. *J. Polym. Sci., Part A* **1964**, *2*, 3857.
(75) G'Sell, C.; Jonas, J. J. *J. Mater. Sci.* **1981**, *16*, 1956.